



Article

The Effect of Liquid-Phase Exfoliated Graphene Film on Neurodifferentiation of Stem Cells from Apical Papilla

Jelena Simonovic¹, Bosko Toljic¹ , Milos Lazarevic¹ , Maja Milosevic Markovic¹, Mina Peric², Jasna Vujin³, Radmila Panajotovic³ and Jelena Milasin^{1,*}

¹ School of Dental Medicine, University of Belgrade, 11000 Belgrade, Serbia

² Center for Laser Microscopy, Faculty of Biology, University of Belgrade, 11000 Belgrade, Serbia

³ Graphene Laboratory, Center for Solid State Physics and New Materials, Institute of Physics, University of Belgrade, 11000 Belgrade, Serbia

* Correspondence: jelena.milasin@stomf.bg.ac.rs

Abstract: Background: Dental stem cells, which originate from the neural crest, due to their easy accessibility might be good candidates in neuro-regenerative procedures, along with graphene-based nanomaterials shown to promote neurogenesis *in vitro*. We aimed to explore the potential of liquid-phase exfoliated graphene (LPEG) film to stimulate the neuro-differentiation of stem cells from apical papilla (SCAP). Methods: The experimental procedure was structured as follows: (1) fabrication of graphene film; (2) isolation, cultivation and SCAP stemness characterization by flowcytometry, multilineage differentiation (osteo, chondro and adipo) and quantitative PCR (qPCR); (3) SCAP neuro-induction by cultivation on polyethylene terephthalate (PET) coated with graphene film; (4) evaluation of neural differentiation by means of several microscopy techniques (light, confocal, atomic force and scanning electron microscopy), followed by neural marker gene expression analysis using qPCR. Results: SCAP demonstrated exceptional stemness, as judged by mesenchymal markers' expression (CD73, CD90 and CD105), and by multilineage differentiation capacity (osteo, chondro and adipo-differentiation). Neuro-induction of SCAP grown on PET coated with graphene film resulted in neuron-like cellular phenotype observed under different microscopes. This was corroborated by the high gene expression of all examined key neuronal markers (Ngn2, NF-M, Nestin, MAP2, MASH1). Conclusions: The ability of SCAPs to differentiate toward neural lineages was markedly enhanced by graphene film.

Keywords: graphene; dental stem cells; stem cells from apical papilla; neurogenic differentiation



Citation: Simonovic, J.; Toljic, B.; Lazarevic, M.; Markovic, M.M.; Peric, M.; Vujin, J.; Panajotovic, R.; Milasin, J. The Effect of Liquid-Phase Exfoliated Graphene Film on Neurodifferentiation of Stem Cells from Apical Papilla. *Nanomaterials* **2022**, *12*, 3116. <https://doi.org/10.3390/nano12183116>

Academic Editors: Jinfeng Zhang, Minhuan Lan and Huiqing Peng

Received: 3 August 2022

Accepted: 5 September 2022

Published: 8 September 2022

Publisher's Note: MDPI stays neutral with regard to jurisdictional claims in published maps and institutional affiliations.



Copyright: © 2022 by the authors. Licensee MDPI, Basel, Switzerland. This article is an open access article distributed under the terms and conditions of the Creative Commons Attribution (CC BY) license (<https://creativecommons.org/licenses/by/4.0/>).

1. Introduction

Regenerative medicine aims at replacing damaged human cells, tissues or organs and restoring their normal architecture and functions [1]. Stem cells (SCs) emerged as a promising tool in regenerative therapies due to their ability to differentiate into numerous cell lineages, high self-renewal capacity and immunosuppressive activity. A variety of new materials and new devices, enhancing cell migration, proliferation, and differentiation, have been developed as well [2,3].

Since SC research has dramatically evolved over the past years, it is possible now to isolate SCs from almost any tissue [4–7]. Yet, in many instances, the most appropriate and matching source of stem cells for a given regenerative therapy remains to be identified.

Dental SCs share a similar origin as neuronal stem cells, as they originate from the neural crest, and due to their accessibility and absence of ethical issues, they might be a good candidate for neuro-regeneration. Apical papilla is a soft tissue at the apex of a not fully formed tooth, containing more than 95% of mesenchymal SCs (stem cells from apical papilla, SCAP) [8,9]. SCAP express some early neural markers even without neural induction and can be transformed into different cell types belonging to neural lineage [10],

making them suitable for potential therapeutic applications in different clinical settings necessitating neuro-repair. SCAP differentiation potential has been extensively tested, but mainly in experiments of osteogenesis and odontogenesis. Only a few studies have dealt with the use of SCAP in neurodifferentiation. For instance, it was shown that fibrin gels [11] and hypoxia [12] stimulate SCAP neurogenesis.

Graphene, an allotrope of carbon, owing to its physico-chemical and biological properties, is also becoming increasingly popular in bioengineering [13–17]. Graphene and graphene-based nanomaterials (GBN), especially graphene oxide, improve cell adhesion during proliferation and differentiation and, due to their electrical conductivity, have the ability to promote the process of differentiation towards neural cells [18–26]. Furthermore, a colloidal dispersion of graphene demonstrated excellent biocompatibility, nontoxicity and remarkable support for cell proliferation [27–31].

As already stated, in numerous studies focusing on tissue engineering, graphene-based materials have been used in conjunction with different dental stem cells, such as dental pulp stem cells, periodontal ligament stem cells and dental follicle stem cells (reviewed by Guazzo et al. [32]). However, differentiation experiments involving graphene derivatives and stem cells from apical papilla are extremely scarce.

Given the lack of studies on SCAP biological behavior when in contact with graphene film, we sought to explore, by means of different microscopy techniques and real-time gene expression analyses, the potential of liquid-phase exfoliated graphene (LPEG) film to induce and stimulate the neuro-differentiation of SCAP.

2. Materials and Methods

The experimental procedure was structured into four phases: phase 1—fabrication of graphene film; phase 2— isolation, cultivation and characterization of stem cells derived from apical papilla; phase 3—seeding stem cells on graphene film and PET; phase 4—evaluation of neural differentiation (Figure 1).

2.1. Fabrication of Graphene Film

2.1.1. Preparation of Graphene Dispersion

The graphene dispersion utilized in this study was prepared by the liquid-phase exfoliation method (LPE) [33]. Following the procedure described in our previous work [34], the mixture was made by adding the graphite powder (Sigma Aldrich-332461) in N-Methyl-2-pyrrolidone (NMP, Sigma Aldrich-328634). The initial concentration was 18 mg/mL. The solution was exposed to ultrasound (Sonic bath, Branson CPXH, Emerson, St. Louis, MO, USA) for 14 h and immediately after the sonication, the graphene dispersion was centrifuged for 60 min at 3000 rpm. The resulting graphene dispersion collected as the top 80% of the supernatant was characterized by UV-VIS spectroscopy (Beckman Coulter DU 720 UV/VIS Spectrophotometer, Brea, CA, USA) [33]. The concentration of LPE graphene dispersion was calculated by Lambert–Beer law [33] and it was 355 $\mu\text{g mL}^{-1}$ (Figure 2).

2.1.2. Liquid-Phase Exfoliated Graphene Film Fabrication

Langmuir–Blodgett technique was applied to transfer graphene thin films from the liquid–gas interface to the solid support substrate [33]. Adding a small amount of liquid-phase exfoliation (LPE) graphene dispersion into the water–air interface, the graphene nanosheets were self-organized into a close-packed film [33]. The thin and transparent film was intently scooped onto the polyethylene terephthalate (PET) substrate. After deposition, the LPE graphene film was left to dry for 20 min in ambient conditions. For the optical characterization of the liquid-phase exfoliated graphene (LPEG) films, UV-VIS spectroscopy (Beckman Coulter DU 720 UV/VIS Spectrophotometer, Brea, CA, USA) was used. The transparence of 80% was estimated for the obtained LPEG film. The transparence of the obtained LPEG film at 550 nm was estimated at 80%, which is consistent with the previously reported study [35].

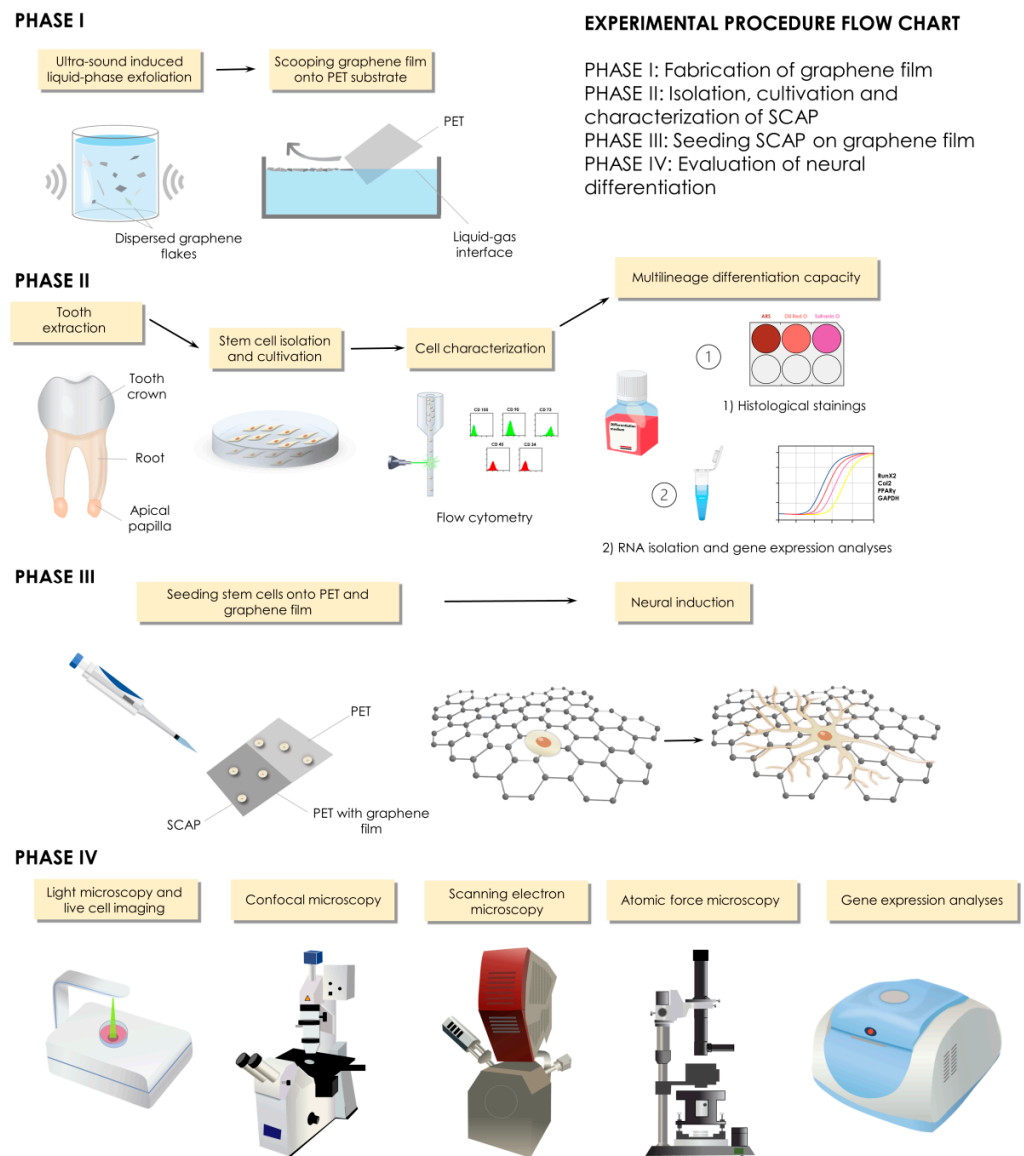


Figure 1. Study design and experimental procedures.

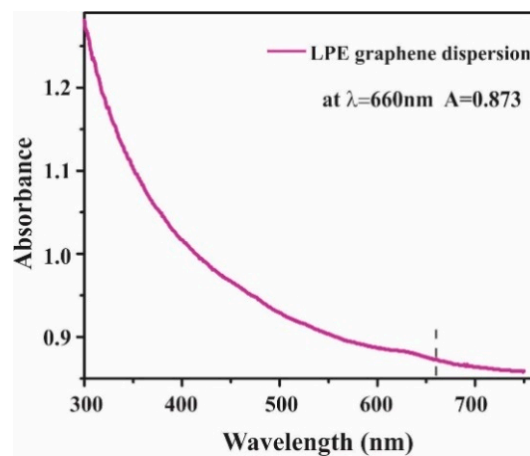


Figure 2. UV-VIS absorption spectrum of LPE graphene dispersion.

2.2. Graphene Film Characterization

2.2.1. Raman Spectroscopy of Graphene Film

Raman spectroscopy, as a noninvasive technique, has been used to provide essential information in the characterization of graphene-based materials [18,19]. Raman spectra were collected with the Micro-Raman Tri Vista 557 triple spectrometer using Nd:YAG laser ($\lambda = 532$ nm) and kept the power below 20 mW to avoid chemical damage of the film induced by the laser heating. The measurements were performed at room temperature and the acquisition time for spectra was 240 s.

2.2.2. Scanning Electron Microscopy (SEM) of Graphene Film

The morphology of the LBA graphene films was characterized with scanning electron microscopy (SEM). SEM images were obtained by Tescan MIRA3 field emission gun SEM working at 20 kV acceleration (Tescan), and SiO₂/Si wafer was used as a substrate.

2.2.3. Atomic Force Microscopy (AFM) of Graphene Film

Graphene film was characterized on an atomic force microscope (AFM), NTEGRA Spectra (NT-MDT). An NT MDT gold-plated tip with a nominal radius of about 30 nm was used. Scans were performed in ambient conditions, RH: 40–50%, t: 23–26 °C in semi-contact mode, with a scan frequency of 0.5 Hz and with 512 × 512 dots in the scan (10 × 10 μm surface). AFM image analysis has been performed using Gwyddion open source software package ver. 2.60 (Prague, Czech Republic). Thickness has been estimated at the edge of the film using profile function and statistical function in the software.

2.3. Cell Cultures

The study was approved by the Ethical Committee of the School of Dental Medicine, University of Belgrade (No 36/19). Immature, impacted third lower molar was extracted from a teenage patient at the Clinic for Oral Surgery (Figure 3), School of Dental Medicine, University of Belgrade, after signing the informed consents by patient's parents. Stem cells from apical papilla were isolated as previously described [34]. Briefly, extracted tooth was rinsed with Dulbecco's Phosphate-Buffered Saline (DPBS, Thermo Fisher Scientific, Waltham, MA, USA), and apical papilla was separated from the root apex and transferred into T-25 flasks after mincing. The tissues were grown in cell complete medium (DMEM supplemented with 10% fetal bovine serum and 1% antibiotic-antimycotic solution). Cells were cultured under standard conditions (37 °C, 95% air–5% CO₂ atmosphere, 95% humidity) and growth medium was changed every third day. All following experiments were carried out with the cells from the fourth and fifth passage.

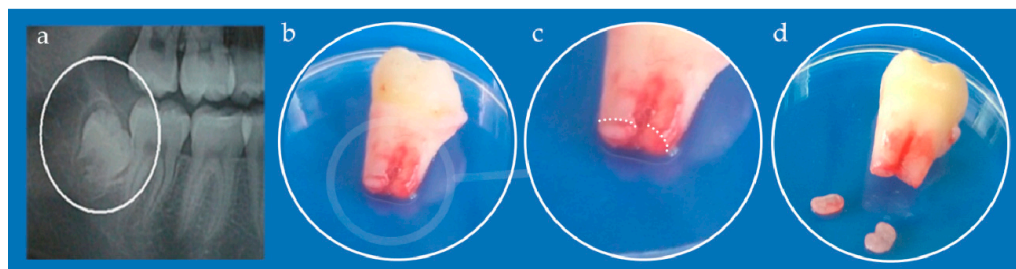


Figure 3. (a) Orthopantomogram of right mandibular impacted third molar (encircled); (b) Extracted tooth; (c) Detail from (b) white dotted line depicts border between apical papilla (lower parts) and tooth root (upper part); (d) Kidney-shaped apical papilla tissues separated from the tooth.

2.4. SCAP Characterization

2.4.1. Flow Cytometry

Flow cytometry analyses were performed in order to assess the expression of specific mesenchymal markers of SCAP. The markers used for these analyses were: fluorescein-

isothiocyanate-labeled mouse monoclonal antibodies against CD90, CD105, and CD34; phycoerythrin-labeled mouse monoclonal antibodies against CD73 and CD45 (all antibodies were purchased from Exbio, Vestec, Czech Republic). Cells were harvested with TrypLE™ Express solution, washed with DPBS supplemented with 10% FBS, and finally counted on automated cell counter Countess™ (Invitrogen, Waltham, MA, USA). One million of the cells were resuspended in 1 mL of 10% FBS solution in DPBS and incubated with adequate antibodies for 45 min in the refrigerator. After incubation, cells were fixed with 4% paraformaldehyde (PFA) for 20 min and finally rinsed 2 times with DPBS. Cells were analyzed on a tabletop flow cytometer (Partec, Munster, Germany) and results were processed by software (FloMax 2.82, Partec, Munster, Germany).

2.4.2. Multilineage Differentiation Capacity

To evaluate the stemness characteristics of SCAP, their potential of differentiation into multiple lineages (osteo-, chondro- and adipo-) was tested. Cells were seeded onto 6-well plates either on PET alone or on PET coated with LPEG film, at density of $5 \times 10^3/\text{cm}^2$, and grown in the respective differentiation medium, which was changed every 2 days. After the required differentiation period of time elapsed, cells from one well were used for RNA isolation for gene expression analysis.

Osteo-Differentiation

After 28 days of culturing in osteo-differentiation medium (StemPro™ Osteogenesis Differentiation Kit, Thermo Fisher Scientific, Waltham, MA, USA) according to manufacturers' recommendations, cells were subjected to histological staining method using Alizarin Red S, as previously described [34]. Briefly, after rinsing with DPBS and fixating with 4% PFA for 30 min, cells were stained with 2% Alizarin Red S (Centrom, Belgrade, Serbia) solution, at pH 4.2. After 30 min of incubation, dye was removed, and cells were rinsed twice with distilled water. Stained cultures were observed using inverted light microscopy (Primovert, Zeiss, Oberkochen, Germany) and photographed.

Chondro-Differentiation

For the chondro-induction, cells were seeded in a form of micromass at total number of 1.5×10^6 and grown on 6-well plates in commercially available chondrogenesis media (StemPro™ Chondrogenesis Differentiation Kit, Thermo Fisher Scientific, Waltham, MA, USA) for 21 days. Chondrogenesis was confirmed by 0.1% solution Safranin O (Centrom, Belgrade, Serbia) positive staining. Stained cells were observed using inverted light microscopy and photographed.

Adipo-Differentiation

Adipogenic stimulation lasted 28 days in commercially available adipogenesis media (StemPro™ Adipogenesis Differentiation Kit, Thermo Fisher Scientific, Waltham, MA, USA) at seeding density of 1×10^4 cells/cm² onto 6-well plates. In order to confirm adipodifferentiation, Oil Red O (Centrom, Belgrade, Serbia) staining was used to visualize intracellular lipid accumulation as lipid vacuoles. Stained cells were observed using inverted light microscopy and photographed.

2.5. LPEG Neuro-Induction

To induce neurogenic differentiation, cells (1.5×10^5) were seeded onto T-25 tissue culture flasks in standard culture medium. After 24 h, neural pre-induction medium and DMEM with 100 mM beta-mercaptoethanol were added, and cells were incubated for 4 h. Then, cell differentiation was continued in a neural induction medium containing recombinant human basic fibroblast growth factor, neural growth factor, and B27 supplement (all from Thermo Fisher Scientific, Waltham, MA, USA) in DMEM either on PET alone or on PET coated with LPEG film. After 7 days of cultivation, cell morphology was observed under inverted microscope. Control cells were incubated in standard culture medium.

2.6. Cell Morphology Analysis Following LPEG Neuro-Induction

2.6.1. Light Microscopy

Cell morphology was observed under inverted microscope (Primover, Zeiss, Oberkochen, Germany) and photographed. Between days 3 and 7 of neurogenic culture, the cells showed a transition from fibroblast-like to neuron-like cell bodies with long processes, suggesting that the stem cells differentiated into neurons/neuron-like cells. At that point they were subjected to RNA isolation, gene expression and immunocytochemistry analysis. In addition, the growth and morphology of the cells during 5 days of LPEG neuro-induction was recorded with CytoSMART Lux 2 camera (CytoSmart Technologies BV, Eindhoven, The Netherlands).

2.6.2. Confocal Microscopy

For the immunocytochemical analyses, cells were seeded onto 25 mm diameter round glass coverslips at density of $5 \times 10^3/\text{cm}^2$ and subjected to neuro-differentiation protocol as described. On the 7th day of neural induction, cells were rinsed 3 times in DPBS, fixed with 4% PFA solution for 20 min, rinsed three times with DPBS and incubated at room temperature for 45 min in blocking and permeabilization buffer (10% Bovine serum albumin and 0.1% Triton X-100 in DPBS). For immunofluorescent detection of neuronal cell marker expression, cells were incubated with the following primary antibodies: rabbit anti- β III-tubulin (B3T, 1:400, Cell Signaling, Danvers, MA, USA), rabbit anti-MAP2 (MAP 1:400, Millipore, Germany) and rabbit anti-neuronal nuclei (NeuN, 1:250, Millipore, Taufkirchen, Germany). Primary antibodies were incubated at 4 °C overnight and subsequently washed 3 times with DPBS. Cell samples were incubated with secondary antibodies—donkey anti-mouse Alexa Fluor 488 (1:200, Invitrogen, Waltham, MA, USA), donkey anti-rabbit Alexa Fluor 555 (1:200, Invitrogen, Waltham, MA, USA) and donkey anti-rabbit Alexa Fluor 657 (1:200, Invitrogen, Waltham, MA, USA) for 2 h in dark at room temperature. Cells were washed 3 times in DPBS and stained with 4-, 6- diamidino- 2-phenylindole (1:4000, DAPI, Molecular Probes, Eugene, OR, USA) for 10 min in dark at room temperature. After washing in DPBS cell samples were mounted with Mowiol(Sigma Aldrich, St. Louis, MO, USA) on microscope slides. Immunofluorescence microscopy images were obtained by confocal laser-scanning microscope (LSM 510, Carl Zeiss GmbH, Jena, Germany) equipped with Ar 488 and HeNe 543 and 633 laser lines. Micrographs were analyzed using Fiji-Image J softwarever 1.46 (NIH, Bethesda, MD, USA).

2.6.3. AFM of Neuron-like Cells

For the purposes of atomic force microscopy, cells had to be seeded on SiO₂ slides coated with a 2 × 2 cm graphene monolayer at a concentration of 200 cells in 10 μL of complete growth medium. The slides were placed in the wells of the 6-well plate. One hour after seeding, 740 μL of complete medium was added to the cells. After 24 h from seeding, neuro-differentiation was performed by the protocol described above.

Seven days after neuro-induction, the medium was aspirated from the well, and the plates were washed twice with DPBS, then the cells were fixed with 4% PFA solution for 20 min. Any excess fixation solution was removed by rinsing twice more with DPBS.

The morphology of the obtained cells after LPEG neuro-differentiation was characterized by microscopy on an atomic force microscope, using the same device and experimental conditions as for the graphene film characterization.

2.6.4. SEM of Neuron-like Cells

After neuro-induction, cell morphology was observed by SEM using a high-resolution electron microscope, MIRA3 FEG-SEM (Tescan, Brno—Kohoutovice, Czech Republic), at a voltage acceleration of 20 kV. Cell fixation using the increasing concentrations of ethanol was done as previously described [36]. In preparation, the sample surface was coated with an ultrathin layer of gold using an SC7620 mini atomizer (Quorum Technologies, Laughton, East Sussex, UK) to prevent the accumulation of static field electricity.

2.7. RNA Isolation and Gene Expression

The expression of different markers was assessed by real-time PCR (qPCR) analysis. RNA was isolated using TRIzol Reagent (Thermo Fisher Scientific, Waltham, MA, USA), according to manufacturers' recommendation. Subsequent reverse transcription from 1 µg of total RNA was performed using RevertAid First Strand cDNA Synthesis Kit (Thermo Fisher Scientific, Waltham, MA, USA) in order to obtain cDNA for qPCR analysis. The list of specific primers is given in Table 1. The results obtained from each qPCR run were threshold cycle (Ct) values. The relative expression level was assessed using the $\Delta\Delta C_t$ method [37]. The relative mRNA expression levels for each sample were calculated as the ratio between the expression of the gene of interest and the expression of the housekeeping gene (GAPDH).

Table 1. Primers with corresponding sequences used in the study.

Primer Name		Sequences (5'→3')
Runx2	Forward	ACAAACAACCACAGAACCACAAGT
	Reverse	GTCTCGGTGGCTGGTAGTGA
Col2	Forward	TTCAGCTATGGAGATGACAATC
	Reverse	AGAGTCCTAGAGTGACTGAG
PPARG	Forward	GCTGTGCAGGAGATCACAGA
	Reverse	GGCTCCATAAAGTCACCAA
Ngn2	Forward	CCTGGAAACCATCTCACTTCA
	Reverse	TACCCAAAGCCAAGAAATGC
NF-M	Forward	TGGGAAATGGCTCGTCATTT
	Reverse	CTTCATGGAAACGGCCAA
Nestin	Forward	AACAGCGACGGAGGTCTCTA
	Reverse	TTCTCTTGTCGCCGAGACTT
MAP2	Forward	AACCCTTTGAGAACACGACA
	Reverse	TCTTTCCGTTTCATCTGCCA
MASH1	Forward	CCAGTTGTACTTCAGCACC
	Reverse	TGCCACTTTGAGTTTGGAC
GAPDH	Forward	TCATGACCACAGTCCATGCCATCA
	Reverse	CCCTGTTGCTGTAGCCAAATTCGT

2.8. Statistical Analysis

GraphPad Prism ver. 9 was used for the analyses (GraphPad Software, Inc., San Diego, CA, USA). After examination of the distribution normality by Kolmogorov–Smirnov normality test, independent sample T tests were performed. The values are presented as mean \pm SD. Statistical significance was set at $p < 0.05$. The experiments were performed in triplicate, repeated at least two times.

3. Results

3.1. Graphene Film Characterization

3.1.1. Raman Spectroscopy of Graphene Film

Raman spectroscopy has been applied to verify the exfoliation of the pristine graphite powder, as bulk material, into few-layer graphene nanosheets. Figure 4 represents the Raman spectra of LPEG thin films and pristine graphite powder as a reference.

D (~1352) and G (~1582) peaks are noted in the same position at both Raman spectra. The changes of shape and Raman shift of 2D peak at Raman spectra of graphene film are evident. A well-defined and sharp shape of the 2D peak, as well as a considerable shift to lower wavenumbers (by 12 cm^{-1}) compared to graphite, are characteristics of a few-layer graphene nanoflakes [24]. D' peak (~1618 cm^{-1}), visible as the shoulder of G peak in the graphene film, together with D peak, confirms the presence of defects and some amount of

disorder in the graphene lattice. The combinations of the main peaks can be also observed: $D + D'$ ($\sim 2939 \text{ cm}^{-1}$) and $D + D''$ ($\sim 2452 \text{ cm}^{-1}$), where the D'' peak is known as a weak defect induced one phonon process.

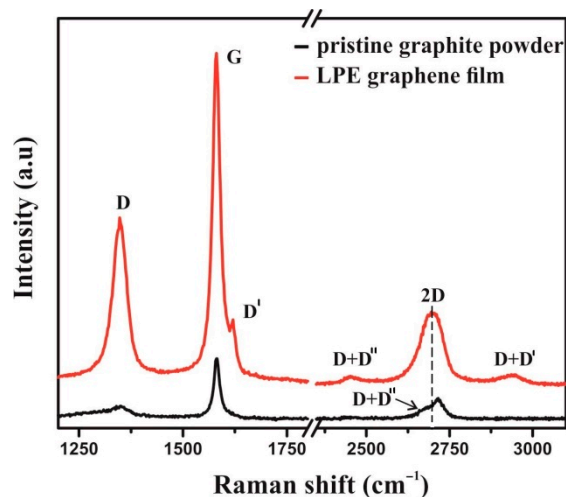


Figure 4. Raman spectrum of LPE graphene film (red line) and pristine graphite powder (black line).

3.1.2. SEM Characterization of Graphene Film

Information about the morphology and film structure was obtained by SEM (Figure 5). The overlapping of the graphene nanosheets and the formation of a closed packed film can be noticed in Figure 5a. Based on the measurement of lateral size, the average diameter of graphene nanosheets was estimated to be in the range of $125 \pm 10 \text{ nm}$ (Figure 5b).

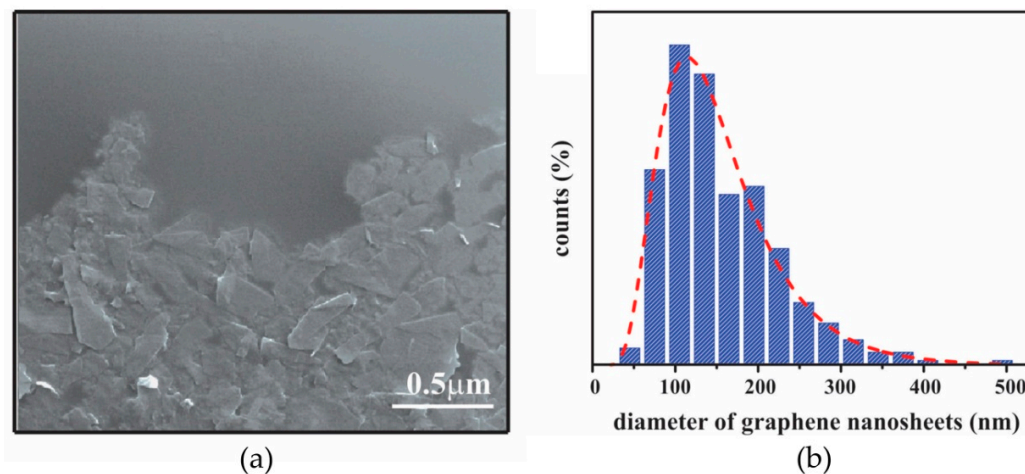


Figure 5. (a) SEM image of graphene film; (b) Histograms of lateral size of graphene nanosheets obtained from six $3 \times 3 \mu\text{m}^2$ SEM images (~ 1800 flakes); The red dashed line represents a log-normal fit.

3.1.3. AFM Characterization of Graphene Film

AFM scans of graphene film along with their characteristics are given in Figure 6. Both 2D (a) and 3D (b) images are shown for a scan area of $20 \times 20 \mu\text{m}$ (512×512 lines), as well as for a scan area of $5 \times 5 \mu\text{m}$ —2D image (c), 3D image (d) and phase image (e). Height distribution for the area of $20 \times 20 \mu\text{m}$ and average height profile across the film are given in Figure 6f,g, respectively.

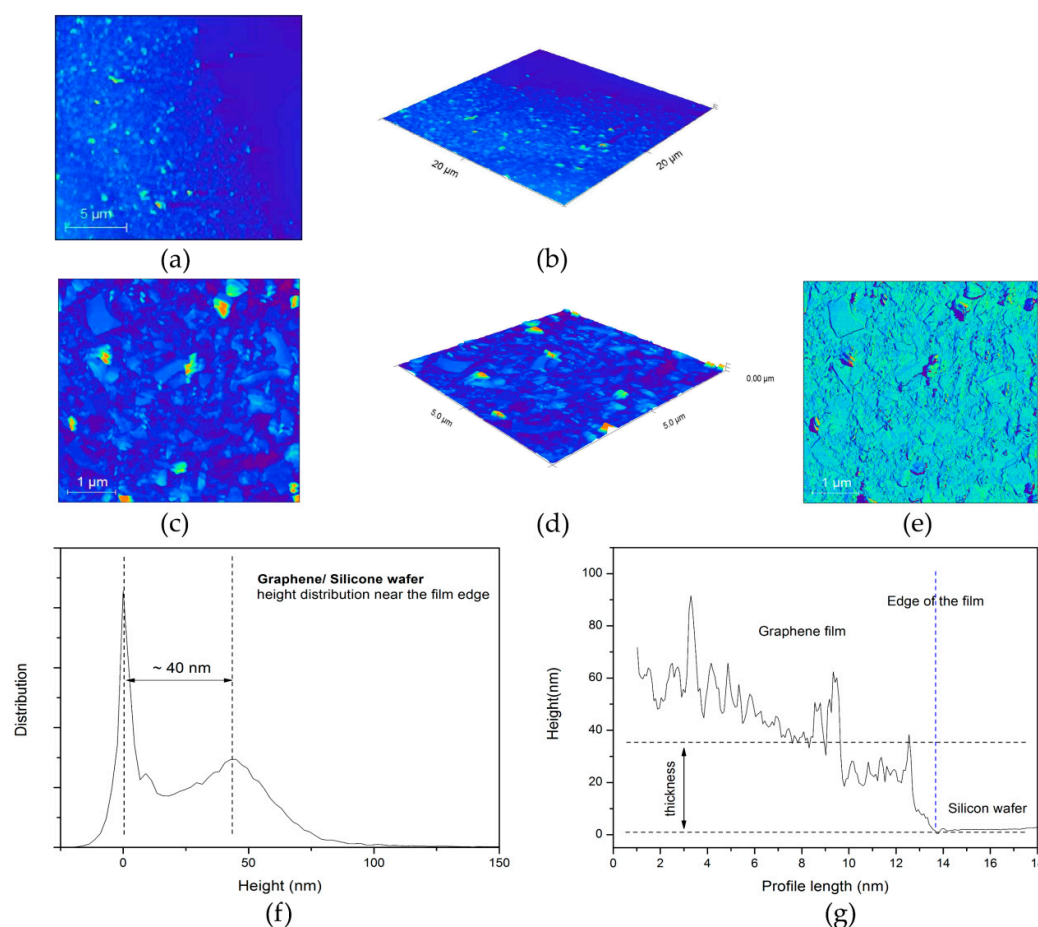


Figure 6. Graphene film near the edge. (a) 2D and (b) 3D image of the scan area $20 \times 20 \mu\text{m}$; (c) 2D, (d) 3D and (e) phase image of the scan area $5 \times 5 \mu\text{m}$; Thickness of graphene film. (f) Height distribution near the edge of the film measured for the area $20 \times 20 \mu\text{m}$ and (g) average height profile across the edge of the film.

3.2. SCAP Characterization

3.2.1. Flow Cytometry Analysis

Flowcytometry analyses were performed on P5 (fifth passage) stem cell from apical papilla. Flowcytometry revealed the expression of mesenchymal stem cell markers CD73, CD90 and CD105 (99%, 91.3% and 96%, respectively), and the absence of hematopoietic markers CD34 (0.34%) and CD45 (0.01%).

3.2.2. Multilineage Differentiation Capacity

Alizarin Red S staining of mineralized nodules around cells confirmed osteogenic differentiation (Figure 7a); the presence of Safranin O clusters of proteoglycans characteristic for cartilage cells confirmed chondro-differentiation (Figure 7b); the presence of Oil Red O staining was indicative of intracellular lipid accumulation (Figure 7c). In the control group (non-induced cells) there were no stained cells (Figure 7d).

3.2.3. Gene Expression Analysis of Multilineage Differentiation

Real-time PCR analysis of gene expression confirmed successful SCAP differentiation, both when cells were grown on graphene film and when they were grown on PET only (control), thus confirming SCAP stemness. Differentiated cells grown on graphene film showed several times higher expression of Runx2—marker of bone tissue (9.59-fold increase), Col2—marker of cartilage tissue (62.90-fold increase) and PPARG—marker of

adipose tissue (17.48-fold increase) compared to the control group (Figure 8), pointing to the positive effect of graphene in terms of its multilineage induction capacity.

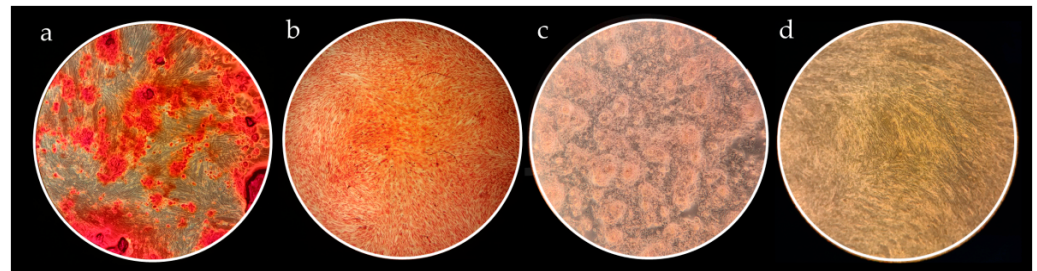


Figure 7. Histological evaluation of SCAP multilineage differentiation capacity. All micrographs were taken at 40× magnification. (a) Alizarin Red S staining of calcium deposits showing osteogenic potential of SCAP; (b) Safranin O staining of proteoglycan aggregates evidencing successful SCAP chondrogenic potential; (c) Oil Red O positive staining of intracellular lipid droplets as a sign of SCAP adipogenic differentiation; (d) Representative image of unstained controls.

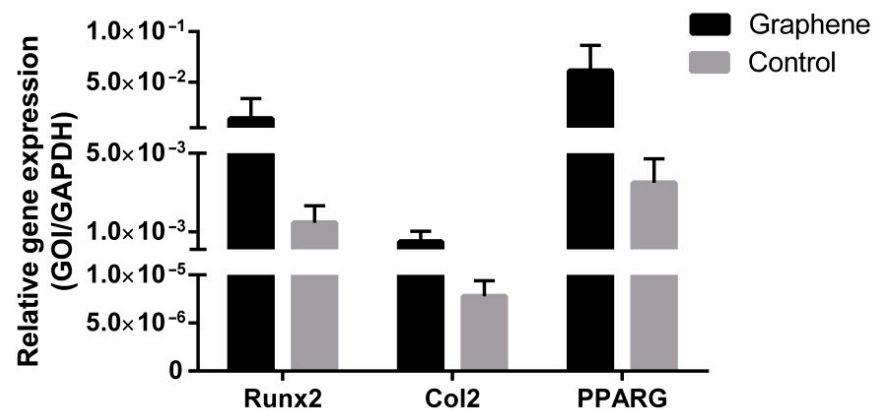


Figure 8. Gene expression evaluation of SCAP osteogenic (Runx2), chondrogenic (Col2) and adipogenic (PPARG) differentiation potential.

3.3. LPEG Neuro-Induction of SCAP

3.3.1. Light Microscopy

After 3–5 days of neuro-induction, cells grown on LPEG film reshaped into polygonal structures with long, slender cytoplasmic processes that were mainly in contact with adjacent cells. Representative light microscopy images of those neuron-like cells are given in Figure 9a–c. While SCAPs on LPEG film gradually changed their morphology into multipolar cells, similar to neurons, cells grown on PET showed minor changes in cell shape (Figure 9d). The growth and morphology of cells during LPEG film neuro-induction were recorded with a CytoSMART Lux 2 camera (CytoSmart Technologies BV, Eindhoven, the Netherlands). A graphical representation of the time-dependent extension of cytoplasmic processes (in μm) is shown in Figure 9e, along with 6 h time frames that were extracted from the video (Figure 9f). The real-time recording of cell morphology changes can be also viewed (Video S1).

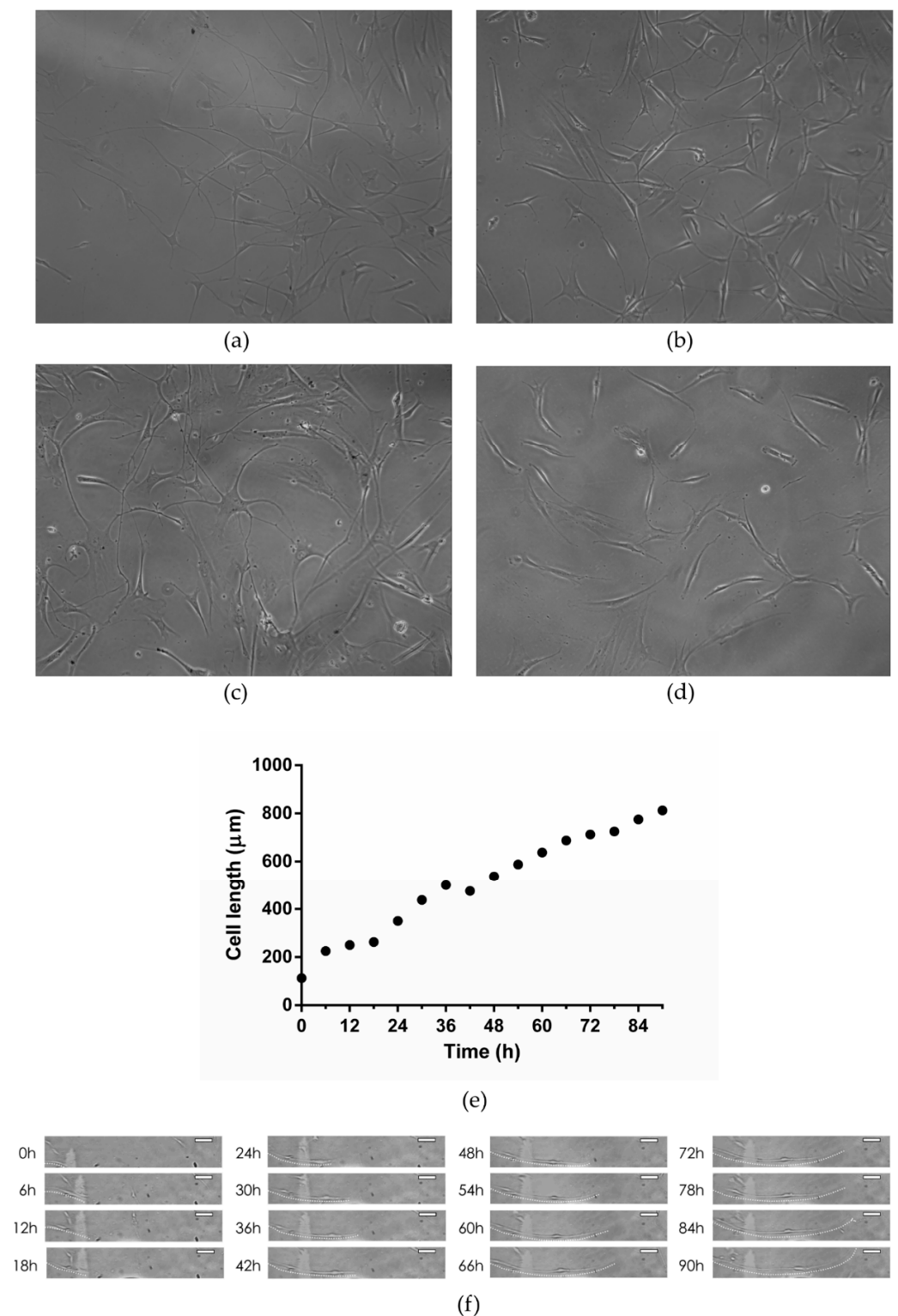


Figure 9. (a–c) Representative light micrographs of SCAP grown on graphene film; (d) Representative light micrograph of SCAP grown on PET; (e) Time-dependent changes in major axis length of SCAP grown on graphene film; (f) Time-lapse light micrographs of SCAP grown on graphene film (dotted white line represents cell extension pathway; white scale bar represents 100 μm).

3.3.2. Confocal Microscopy

Confocal microscopy showed the increased expression of three major neural cell markers (NeuN, MAP2 and β -3 tubulin) in SCAPs grown on graphene, compared to cells grown on PET alone (control) (Figure 10).

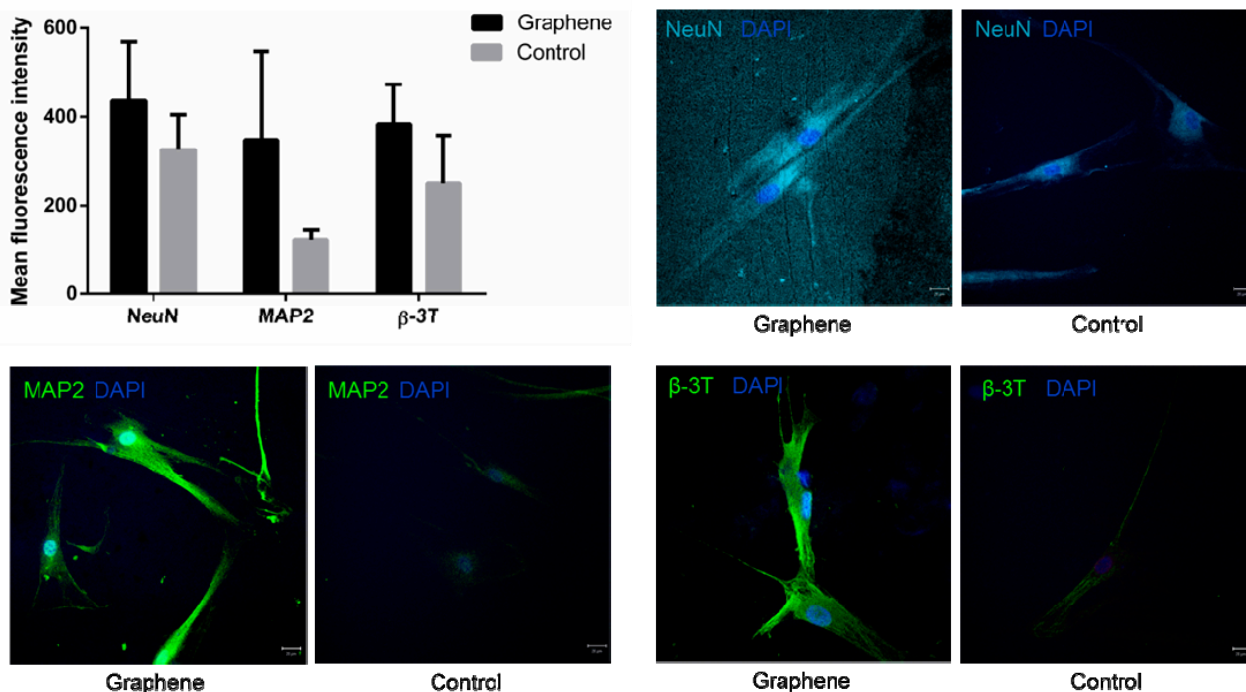


Figure 10. Mean fluorescence intensities and laser confocal micrographs of SCAP immunolabeled for neuronal markers NeuN, MAP2 and β -3-tubulin (nuclei are labeled with DAPI).

3.3.3. AFM of Neuron-like Cells

Atomic force microscopy (AFM) revealed subtle surface topography and morphological differences between stem cells grown on graphene film compared to those placed over PET. SCAP grown on graphene were polygonal in shape (Figure 11a,b) with multiple long-distance, slender cytoplasmic projections emerging from cell body (Figure 11c,d) compared to the less complex cell morphology of SCAP grown on PET (Figure 11e,f). Note that AFM height panel also revealed numerous globular protrusions on the surface of the cell bodies, which were more present on SCAP grown on graphene.

3.3.4. SEM of Neuron-like Cells

Scanning electron microscopy (SEM) of SCAP grown on graphene film depicted a triangular cell body with long, slender projections (Figure 12a). The endings of these projections were in close proximity or direct contact with cytoplasmic projections of surrounding cells forming a connected cell population (Figure 12b).

3.3.5. Gene Expression Analysis after LPEG Neuro-Induction

Gene expression analysis of key neural differentiation markers of SCAP grown on LPEG film and control material is presented in Figure 13. All examined markers showed higher expression in cells grown on graphene film compared to those on non-coated PET (control).

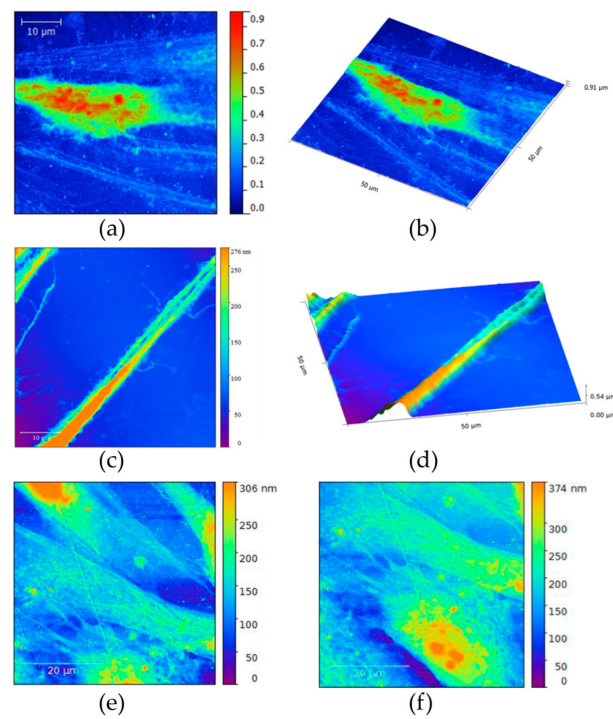


Figure 11. (a,b) Atomic force micrographs of SCAP grown on graphene film; (c,d) Long, slender projections of SCAP cell membrane covering graphene film; (e,f) AFMs of control SCAP grown on PET (control).

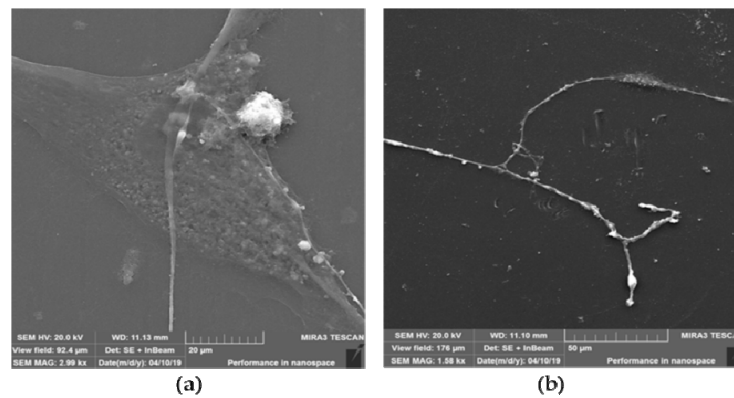


Figure 12. SEM of SCAP grown on graphene film. (a) Triangular cell body with arising long-distance membrane projections; (b) Slender cell projections synapsing with adjacent cell.

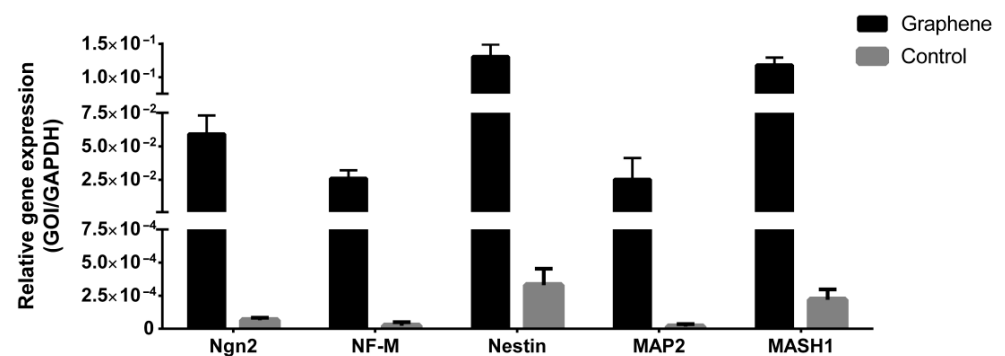


Figure 13. Gene expression analyses of neuronal markers of SCAP grown on graphene film and PET (control).

4. Discussion

Many dental tissues are precious niches of mesenchymal stem cells that are becoming increasingly appealing in regenerative medicine due to their easy accessibility and lack of health risks for the donor. They are especially attractive for the field of neuro-regeneration given that they originate from the neural crest and possess the capacity of differentiation into diverse neural cell types. Apical papilla, the soft tissue at the apex of a not fully formed tooth, contains a very high percentage of MSCs characterized by great plasticity, proliferation rate and differentiation ability. Previous studies, based on immunophenotyping, gene expression analyses, and patch clamping, have reported that SCAP grown under neural inductive conditions could give rise to a variety of neural cell phenotypes, from neuroprogenitors to mature neurons [10,34].

The number of novel materials used as cell carriers/scaffolds, tested for tissue engineering application, is constantly increasing, especially in the field of neuro-repair and regeneration. Great emphasis has been put on carbon nanostructured scaffolds that may display suitable characteristics for neural differentiation [13,34,38,39]. Graphene nanomaterials are carbon crystal allotropes with a two-dimensional structure and, according to data from the literature, have proven to be an excellent nanomaterial for neurodifferentiation due to their unique organization, chemical stability, exceptional mechanical properties, bactericidal potential, and biocompatibility [40,41]. This monoatomic layer of carbon shows the ability to absorb growth factors and exhibits electrical conductivity, which is of particular interest for the field of neuroscience. For instance, Lee et al. have convincingly demonstrated, on a neuroblastoma cell line, that graphene substrate enhanced neurite outgrowth, both in terms of length and number [42]. Rodrigues-Losada et al. also showed that different graphene materials (graphene oxide and reduced derivatives) promoted the differentiation, proliferation and maturation of dopaminergic neurons [43]. Importantly, graphene-based materials also exert stimulating effect on cell differentiation towards neurons rather than glial cells [44]. In neural regeneration, the induction of stem cell differentiation in favor of neurons against glial cells is highly desirable, making graphene-based nanomaterials a promising agent in neuroregenerative therapies. In addition to graphene oxide, the most studied graphene nanomaterial, there are other forms of graphene that are non-toxic and biocompatible, such as fully reduced or partially reduced graphene oxide, in the form of powder or film, but their positive effects in terms of neurodifferentiation have not yet been sufficiently investigated. This is the case with liquid-phase exfoliated graphene (LPEG) film that was the subject of this research. In the present study, Raman spectroscopy has been applied to verify the exfoliation of the pristine graphite powder, as bulk material, into graphene nanosheets. Indeed, the obtained closed packed film was made of few-layer graphene nanoflakes, as seen on SEM. The changes of shape and Raman shift of the 2D peak at Raman spectra of graphene film are evident. A well-defined and sharp shape of the 2D peak as well as a considerable shift to lower wave number compared to graphite are characteristics of few-layer graphene nanoflakes [45]. Edge defects, as the dominant type of defect in graphene film, are the result of the cavitation process at the liquid phase exfoliated technique [46]. Generally, the Raman spectra as well as the average diameter of the nanosheets and their height were in agreement with some previous reports [47].

In the present study, the mandatory characterization of SCAP cultures has shown a highly predominant presence of cells displaying mesenchymal stem cell markers (between 91 and 99% of cells in the culture expressed a given mesenchymal marker). Concomitantly, a negligible percentage of cells expressed hematopoietic stem cell markers (only 0.01% and 0.34% of cells expressed CD45 and CD34, respectively), as determined by flowcytometry, pointing to the fact that cell cultures contained principally MSCs. Similarly, stemness characterization by means of multiple lineages induction showed a successful osteo-, chondro- and adipo-differentiation of SCAPs. The specific osteo-, chondro- and adipo cellular phenotypes, assessed by appropriate staining procedures, were also confirmed by high mRNA levels of selected markers (Runx2, Col2 and PPARG, for osteo-, chondro- and adipo-differentiation, respectively). These findings are in general agreement with some

previous reports [48–50]. Interestingly, the three examined processes of differentiation also appeared to be enhanced in the presence of graphene (especially chondrogenesis) but more markers specific for osteo-, chondro- and adipo- lineages should be evaluated in order to confirm that positive effect of graphene film. This is in line with some previous studies. Namely, it was found that graphene derivatives exhibit great stimulatory effects on adipogenesis and osteogenesis [19,51–53], pointing to the possibility of their use in composite tissue cultures when more than one cell type is needed. This is of utmost importance in regenerative medicine and dentistry when huge defects require complex reconstructions. The classical example is the surgical removal of a portion of maxilla or mandible in cases of oral cancer, resulting in massive bone, muscle and nerve defects, which necessitate multiple tissues' replacement.

Regarding neurogenesis, the present study showed for the first time that LPEG films can have strong stimulatory effects on SCAPs' induction towards neural lineage. Namely, cells cultured in neurodifferentiation medium on graphene film demonstrated increased levels of all neural markers (studied either by confocal microscopy or by quantitative PCR), compared to cells grown in neurodifferentiation medium only. The levels of *ngn-2*, an inhibitor of glial cell transcription factor, were very high, indicative of LPEG capacity to suppress gliogenesis, thus favoring neurogenesis [54]. Gene expression of Nestin, a marker of neuroepithelial and radial cells, was, as well, increased in cells grown on graphene film compared to those seeded over the non-coated substrate. This protein has a crucial role in assembling and disassembling intermediate filaments and thus maintains the structure and regulates the growth of developing neural cells [55]. Similarly, a higher expression of Mash-1, a marker of intermediate progenitors, was also noted. Mash-1, as one of the early markers that determine cellular fate, is involved in the differentiation of neuroblasts, as well as in cell protection mechanisms that prevent cell damage and apoptosis. β III-tubulin, a neuronal microtubule protein that is particularly expressed during neurogenesis and is thought to be responsible for axon growth, was upregulated in the presence of graphene. The level of MAP2, a cytoskeletal element essential for the binding and stabilization of neuronal microtubules with major impact on neuronal development, was also higher in cells grown on graphene film [56]. Another neural marker of mature neurons that has never been found in glial cells—NeuN—was more expressed in SCAP stimulated by LPEG compared to the control condition. This marker was detected, both in the cell nucleus and perinuclear cytoplasm. Unlike the nuclear form, which binds to DNA and most probably has an important role in the regulation of neurogenesis, the role of the cytoplasmatic variant is still unclear. It is assumed that, together with Synapsin I, cytoplasmatic NeuN regulates the mobility of synaptic vesicles and release of neurotransmitters, thus playing a potential role in synaptogenesis and establishing neural circuits [57]. The last examined, final stage marker of neural development, along with MAP2 and NeuN, was Neurofilament Medium (NF-M) and, again, its expression was higher in cells grown on graphene. In agreement with our findings, which showed positive effects of graphene film on neurogenesis, a previous study that examined several types of graphene material established that the morphology of the film and the species of graphene influenced the behavior of neurons, but generally film species exhibited higher biocompatibility than powder materials [43]. Our results support the central concept of graphene substrates' beneficial effects on the neural induction of several types of mesenchymal stem cells [58].

Future studies testing the neuroinductive capacity of graphene should use films with different physico-chemical characteristics along with other stem cells of dental origin, such as pulp or follicle cells, combined with different culture media. In addition, markers' quantification at the protein level should rely on ELISA or Westernblot analyses as more precise than immunofluorescence quantification, thus overcoming some limitations of this study.

5. Conclusions

The predisposition of SCAPs to differentiate toward neural lineages, as well as the neuroinductive properties of graphene film, should warrant further studies of dental stem cells in conjunction with this nanomaterial, with the aim of finding an optimal solution for autologous neuroregenerative therapy.

Supplementary Materials: The following supporting information can be downloaded at: <https://www.mdpi.com/article/10.3390/nano12183116/s1>, Video S1: Time-dependent changes in morphology of SCAP grown on LPEG film.

Author Contributions: Conceptualization, J.S. and J.M.; methodology, J.S., R.P. and J.M.; validation, J.M.; formal analysis, J.S., B.T., M.L. and M.M.M.; investigation, J.S., B.T., M.L., M.M.M., M.P. and J.V.; resources, R.P. and J.M.; data curation, J.S., M.P. and J.V.; writing—original draft preparation, J.S.; writing—review and editing, M.L., M.M.M. and J.M.; visualization, B.T. and M.L.; supervision, J.M.; project administration, J.M.; funding acquisition, J.M. All authors have read and agreed to the published version of the manuscript.

Funding: This research was supported by the Ministry of Education, Science and Technological Development of the Republic of Serbia grant number 451-03-9/2021-14/200129 and by the Science Fund of the Republic of Serbia, #GRANT No 7750038, ORAL CANCER—NEW APPROACHES IN PREVENTION, CONTROL AND POST-OPERATIVE REGENERATION—AN IN VIVO STUDY—ORCA-PCR.

Institutional Review Board Statement: The study was conducted in accordance with the Declaration of Helsinki, and approved by the Ethics Committee of the School of Dental Medicine, University of Belgrade (No 36/19, 19.04.2016).

Informed Consent Statement: Informed consent was obtained from all subjects involved in the study.

Data Availability Statement: Not applicable.

Acknowledgments: We extend our appreciation to Djordje Miljkovic from the Institute of Biological Research Sinisa Stankovic, University of Belgrade, for the flowcytometry analyses.

Conflicts of Interest: The authors declare no conflict of interest. The funders had no role in the design of the study; in the collection, analyses, or interpretation of data; in the writing of the manuscript; or in the decision to publish the results.

References

1. Mitrečić, D.; Hribljan, V.; Jagečić, D.; Isaković, J.; Lamberto, F.; Horánszky, A.; Zana, M.; Foldes, G.; Zavan, B.; Pivoriūnas, A.; et al. Regenerative Neurology and Regenerative Cardiology: Shared Hurdles and Achievements. *Int. J. Mol. Sci.* **2022**, *23*, 855. [[CrossRef](#)]
2. Liu, A.; Long, Y.; Li, J.; Gu, L.; Karim, A.; Wang, X.; Gibson, A.L.F. Accelerated complete human skin architecture restoration after wounding by nanogenerator-driven electrostimulation. *J. Nanobiotechnol.* **2021**, *19*, 280. [[CrossRef](#)] [[PubMed](#)]
3. Long, Y.; Wei, H.; Li, J.; Yao, G.; Yu, B.; Ni, D.; Gibson, A.L.; Lan, X.; Jiang, Y.; Cai, W.; et al. Effective Wound Healing Enabled by Discrete Alternative Electric Fields from Wearable Nanogenerators. *ACS Nano* **2018**, *12*, 12533–12540. [[CrossRef](#)] [[PubMed](#)]
4. Vishwakarma, A.; Sharpe, P.; Shi, S.; Ramalingam, M. (Eds.) *Stem Cell Biology and Tissue Engineering in Dental Sciences*; Elsevier: Amsterdam, The Netherlands, 2014.
5. Egusa, H.; Iida, K.; Kobayashi, M.; Lin, T.Y.; Zhu, M.; Zuk, P.A.; Wang, C.J.; Thakor, D.K.; Hedrick, M.H.; Nishimura, I. Downregulation of extracellular matrix-related gene clusters during osteogenic differentiation of human bone marrow- and adipose tissue-derived stromal cells. *Tissue Eng.* **2007**, *13*, 2589–2600. [[CrossRef](#)] [[PubMed](#)]
6. Ding, D.C.; Shyu, W.C.; Lin, S.Z. Mesenchymal stem cells. *Cell Transplant.* **2011**, *20*, 5–14. [[CrossRef](#)]
7. Fernandes, K.J.; McKenzie, I.A.; Mill, P.; Smith, K.M.; Akhavan, M.; Barnabé-Heider, F.; Biernaskie, J.; Juneak, A.; Kobayashi, N.R.; Toma, J.G.; et al. A dermal niche for multipotent adult skin-derived precursor cells. *Nat. Cell Biol.* **2004**, *6*, 1082–1093. [[CrossRef](#)]
8. Sonoyama, W.; Liu, Y.; Fang, D.; Yamaza, T.; Seo, B.M.; Zhang, C.; Liu, H.; Gronthos, S.; Wang, C.Y.; Wang, S.; et al. Mesenchymal stem cell-mediated functional tooth regeneration in swine. *PLoS ONE* **2006**, *1*, e79. [[CrossRef](#)]
9. Huang, G.T.; Sonoyama, W.; Liu, Y.; Liu, H.; Wang, S.; Shi, S. The hidden treasure in apical papilla: The potential role in pulp/dentin regeneration and bioroot engineering. *J. Endod.* **2008**, *34*, 645–651. [[CrossRef](#)]
10. Abe, S.; Yamaguchi, S.; Amagasa, T. Multilineage Cells from Apical Pulp of Human Tooth with Immature Apex. *Oral. Sci. Int.* **2007**, *4*, 45–48. [[CrossRef](#)]

11. Germain, L.; De Berdt, P.; Vanacker, J.; Leprince, J.; Diogenes, A.; Jacobs, D.; Vandermeulen, G.; Bouzin, C.; Pr eat, V.; Dupont-Gillain, C.; et al. Fibrin hydrogels to deliver dental stem cells of the apical papilla for regenerative medicine. *Regen. Med.* **2015**, *10*, 153–167. [[CrossRef](#)]
12. Vanacker, J.; Viswanath, A.; De Berdt, P.; Everard, A.; Cani, P.D.; Bouzin, C.; Feron, O.; Diogenes, A.; Leprince, J.G.; des Rieux, A. Hypoxia modulates the differentiation potential of stem cells of the apical papilla. *J. Endod.* **2014**, *40*, 1410–1418. [[CrossRef](#)] [[PubMed](#)]
13. Wang, Y.; Li, Z.; Wang, J.; Li, J.; Lin, Y. Graphene and graphene oxide: Biofunctionalization and applications in biotechnology. *Trends Biotechnol.* **2011**, *29*, 205–212. [[CrossRef](#)] [[PubMed](#)]
14. Lee, W.C.; Lim, C.H.; Shi, H.; Tang, L.A.; Wang, Y.; Lim, C.T.; Loh, K.P. Origin of enhanced stem cell growth and differentiation on graphene and graphene oxide. *ACS Nano* **2011**, *5*, 7334–7341. [[CrossRef](#)] [[PubMed](#)]
15. La, W.G.; Park, S.; Yoon, H.H.; Jeong, G.J.; Lee, T.J.; Bhang, S.H.; Han, J.Y.; Char, K.; Kim, B.S. Delivery of a therapeutic protein for bone regeneration from a substrate coated with graphene oxide. *Small* **2013**, *9*, 4051–4060. [[CrossRef](#)] [[PubMed](#)]
16. Lee, Y.J.; Seo, T.H.; Lee, S.; Jang, W.; Kim, M.J.; Sung, J.S. Neuronal differentiation of human mesenchymal stem cells in response to the domain size of graphene substrates. *J. Biomed. Mater. Res. A* **2018**, *106*, 43–51. [[CrossRef](#)]
17. Mousavi, S.M.; Yousefi, K.; Hashemi, S.A.; Afsa, M.; Bahrani, S.; Gholami, A.; Ghahramani, Y.; Alizadeh, A.; Chiang, W.H. Renewable Carbon Nanomaterials: Novel Resources for Dental Tissue Engineering. *Nanomaterials* **2021**, *11*, 2800. [[CrossRef](#)]
18. Bressan, E.; Ferroni, L.; Gardin, C.; Sbricoli, L.; Gobbato, L.; Ludovichetti, F.S.; Tocco, I.; Carraro, A.; Piattelli, A.; Zavan, B. Graphene based scaffolds effects on stem cells commitment. *J. Transl. Med.* **2014**, *12*, 296. [[CrossRef](#)] [[PubMed](#)]
19. Park, S.Y.; Park, J.; Sim, S.H.; Sung, M.G.; Kim, K.S.; Hong, B.H.; Hong, S. Enhanced differentiation of human neural stem cells into neurons on graphene. *Adv. Mater.* **2011**, *23*, 263–267. [[CrossRef](#)]
20. Wang, Y.; Lee, W.C.; Manga, K.K.; Ang, P.K.; Lu, J.; Liu, Y.P.; Lim, C.T.; Loh, K.P. Fluorinated graphene for promoting neuro-induction of stem cells. *Adv. Mater.* **2012**, *24*, 4285–4290. [[CrossRef](#)]
21. Tang, M.; Song, Q.; Li, N.; Jiang, Z.; Huang, R.; Cheng, G. Enhancement of electrical signaling in neural networks on graphene films. *Biomaterials* **2013**, *34*, 6402–6411. [[CrossRef](#)]
22. Hong, S.W.; Lee, J.H.; Kang, S.H.; Hwang, E.Y.; Hwang, Y.S.; Lee, M.H.; Han, D.W.; Park, J.C. Enhanced neural cell adhesion and neurite outgrowth on graphene-based biomimetic substrates. *Biomed. Res. Int.* **2014**, *2014*, 212149. [[CrossRef](#)] [[PubMed](#)]
23. Bellet, P.; Gasparotto, M.; Pressi, S.; Fortunato, A.; Scapin, G.; Mba, M.; Menna, E.; Filippini, F. Graphene-Based Scaffolds for Regenerative Medicine. *Nanomaterials* **2021**, *11*, 404. [[CrossRef](#)] [[PubMed](#)]
24. Zare, P.; Aleemardani, M.; Seifalian, A.; Bagher, Z.; Seifalian, A.M. Graphene Oxide: Opportunities and Challenges in Biomedicine. *Nanomaterials* **2021**, *11*, 1083. [[CrossRef](#)] [[PubMed](#)]
25. Sanchez, V.C.; Jachak, A.; Hurt, R.H.; Kane, A.B. Biological interactions of graphene-family nanomaterials: An interdisciplinary review. *Chem. Res. Toxicol.* **2012**, *25*, 15–34. [[CrossRef](#)] [[PubMed](#)]
26. Kempainen, J.M.; Hollister, S.J. Tailoring the mechanical properties of 3D-designed poly (glycerol sebacate) scaffolds for cartilage applications. *J. Biomed. Mater. Res. A* **2010**, *94*, 9–18. [[CrossRef](#)]
27. Nair, M.; Nancy, D.; Krishnan, A.G.; Anjusree, G.S.; Vadukumpully, S.; Nair, S.V. Graphene oxide nanoflakes incorporated gelatin-hydroxyapatite scaffolds enhance osteogenic differentiation of human mesenchymal stem cells. *Nanotechnology* **2015**, *26*, 161001. [[CrossRef](#)]
28. Lee, T.J.; Park, S.; Bhang, S.H.; Yoon, J.K.; Jo, I.; Jeong, G.J.; Hong, B.H.; Kim, B.S. Graphene enhances the cardiomyogenic differentiation of human embryonic stem cells. *Biochem. Biophys. Res. Commun.* **2014**, *452*, 174–180. [[CrossRef](#)]
29. Chaudhuri, B.; Bhadra, D.; Moroni, L.; Pramanik, K. Myoblast differentiation of human mesenchymal stem cells on graphene oxide and electrospun graphene oxide-polymer composite fibrous meshes: Importance of graphene oxide conductivity and dielectric constant on their biocompatibility. *Biofabrication* **2015**, *7*, 015009. [[CrossRef](#)]
30. Ay an-Varela, M.; Villar-Rodil, S.; Paredes, J.I.; Munuera, J.M.; Pag an, A.; Lozano-P erez, A.A.; Cenis, J.L.; Mart inez-Alonso, A.; Tasc on, J.M. Investigating the Dispersion Behavior in Solvents, Biocompatibility, and Use as Support for Highly Efficient Metal Catalysts of Exfoliated Graphitic Carbon Nitride. *ACS Appl. Mater. Interfaces* **2015**, *7*, 24032–24045. [[CrossRef](#)]
31. Gopinathan, J.; Quigley, A.F.; Bhattacharyya, A.; Padhye, R.; Kapsa, R.M.; Nayak, R.; Shanks, R.A.; Houshyar, S. Preparation, characterisation, and in vitro evaluation of electrically conducting poly(ϵ -caprolactone)-based nanocomposite scaffolds using PC12 cells. *J. Biomed. Mater. Res. A* **2016**, *104*, 853–865. [[CrossRef](#)]
32. Guazzo, R.; Gardin, C.; Bellin, G.; Sbricoli, L.; Ferroni, L.; Ludovichetti, F.S.; Piattelli, A.; Antoniac, I.; Bressan, E.; Zavan, B. Graphene-Based Nanomaterials for Tissue Engineering in the Dental Field. *Nanomaterials* **2018**, *8*, 349. [[CrossRef](#)]
33. Matkovi c, A.; Milo evi c, I.; Mili evi c, M.; Toma evi c-Ili c, T.; Pe i c, J.; Musi c, M.; Spasenovi c, M.; Jovanovi c, D.; Vasi c, B.; Deeks, C.; et al. Enhanced sheet conductivity of Langmuir–Blodgett assembled graphene thin films by chemical doping. *2D Mater.* **2016**, *3*, 015002. [[CrossRef](#)]
34. Simonovic, J.; Toljic, B.; Nikolic, N.; Peric, M.; Vujan, J.; Panajotovic, R.; Gajic, R.; Bekyarova, E.; Cataldi, A.; Parpura, V.; et al. Differentiation of stem cells from apical papilla into neural lineage using graphene dispersion and single walled carbon nanotubes. *J. Biomed. Mater. Res. A* **2018**, *106*, 2653–2661. [[CrossRef](#)] [[PubMed](#)]
35. Milo evi c, I.R.; Vasi c, B.; Matkovi c, A.; Vujan, J.; A krabi c, S.; Kratzer, M.; Griesser, T.; Teichert, C.; Gaji c, R. Single-step fabrication and work function engineering of Langmuir–Blodgett assembled few-layer graphene films with Li and Au salts. *Sci. Rep.* **2020**, *10*, 8476. [[CrossRef](#)] [[PubMed](#)]

36. Shehadat, S.A.; Gorduysus, M.O.; Hamid, S.S.A.; Abdullah, N.A.; Samsudin, A.R.; Ahmad, A. Optimization of scanning electron microscope technique for amniotic membrane investigation: A preliminary study. *Eur. J. Dent.* **2018**, *12*, 574–578. [[CrossRef](#)]
37. Livak, K.J.; Schmittgen, T.D. Analysis of relative gene expression data using real-time quantitative PCR and the 2^{(-Delta Delta C(T))} Method. *Methods* **2001**, *25*, 402–408. [[CrossRef](#)]
38. Han, F.; Ma, X.; Zhai, Y.; Cui, L.; Yang, L.; Zhu, Z.; Hao, Y.; Cheng, G. Strategy for Designing a Cell Scaffold to Enable Wireless Electrical Stimulation for Enhanced Neuronal Differentiation of Stem Cells. *Adv. Healthc. Mater.* **2021**, *10*, 2100027. [[CrossRef](#)]
39. Madanagopal, T.T.; Tai, Y.K.; Lim, S.H.; Fong, C.H.; Cao, T.; Rosa, V.; Franco-Obregón, A. Pulsed electromagnetic fields synergize with graphene to enhance dental pulp stem cell-derived neurogenesis by selectively targeting TRPC1 channels. *Eur. Cells Mater.* **2021**, *41*, 216–232. [[CrossRef](#)]
40. Zhang, Q.; Zhang, Z.; Yin, J. Free-Standing Buckle-Delaminated 2D Organic Nanosheets with Enhanced Mechanical Properties and Multifunctionality. *Adv. Mater. Interfaces* **2019**, *6*, 1900561. [[CrossRef](#)]
41. Hung, H.S.; Kung, M.L.; Chen, F.C.; Ke, Y.C.; Shen, C.C.; Yang, Y.C.; Tang, C.M.; Yeh, C.A.; Hsieh, H.H.; Hsu, S.H. Nanogold-Carried Graphene Oxide: Anti-Inflammation and Increased Differentiation Capacity of Mesenchymal Stem Cells. *Nanomaterials* **2021**, *11*, 2046. [[CrossRef](#)]
42. Lee, J.S.; Lipatov, A.; Ha, L.; Shekhirev, M.; Andalib, M.N.; Sinitiskii, A.; Lim, J.Y. Graphene substrate for inducing neurite outgrowth. *Biochem. Biophys. Res. Commun.* **2015**, *460*, 267–273. [[CrossRef](#)] [[PubMed](#)]
43. Rodriguez-Losada, N.; Wendelbob, R.; Ocaña, M.C.; Casares, A.D.; Guzman de Villoria, R.; Aguirre Gomez, J.A.; Arraez, M.A.; Gonzalez-Alegre, P.; Medina, M.A.; Arenas, E.; et al. Graphene Oxide and Reduced Derivatives, as Powder or Film Scaffolds, Differentially Promote Dopaminergic Neuron Differentiation and Survival. *Front. Neurosci.* **2020**, *14*, 570409. [[CrossRef](#)] [[PubMed](#)]
44. Chen, L.; Wang, W.; Lin, Z.; Lu, Y.; Chen, H.; Li, B.; Li, Z.; Xia, H.; Li, L.; Zhang, T. Conducting molybdenum sulfide/graphene oxide/polyvinyl alcohol nanocomposite hydrogel for repairing spinal cord injury. *J. Nanobiotechnol.* **2022**, *20*, 210. [[CrossRef](#)] [[PubMed](#)]
45. Ferrari, A.C.; Meyer, J.C.; Scardaci, V.; Casiraghi, C.; Lazzeri, M.; Mauri, F.; Piscanec, S.; Jiang, D.; Novoselov, K.S.; Roth, S.; et al. Raman spectrum of graphene and graphene layers. *Phys. Rev. Lett.* **2006**, *97*, 187401. [[CrossRef](#)] [[PubMed](#)]
46. Bracamonte, M.V.; Lacconi, G.I.; Urreta, S.E.; Torres, L.E.F.F. On the Nature of Defects in Liquid-phase Exfoliated Graphene. *J. Phys. Chem. C* **2014**, *118*, 15455–15459. [[CrossRef](#)]
47. Amaro-Gahete, J.; Benítez, A.; Otero, R.; Esquivel, D.; Jiménez-Sanchidrián, C.; Morales, J.; Caballero, Á.; Romero-Salguero, F.J. A Comparative Study of Particle Size Distribution of Graphene Nanosheets Synthesized by an Ultrasound-Assisted Method. *Nanomaterials* **2019**, *9*, 152. [[CrossRef](#)]
48. Qu, G.; Li, Y.; Chen, L.; Chen, Q.; Zou, D.; Yang, C.; Zhou, Q. Comparison of Osteogenic Differentiation Potential of Human Dental-Derived Stem Cells Isolated from Dental Pulp, Periodontal Ligament, Dental Follicle, and Alveolar Bone. *Stem. Cells Int.* **2021**, *2021*, 6631905. [[CrossRef](#)]
49. Son, Y.B.; Kang, Y.H.; Lee, H.J.; Jang, S.J.; Bharti, D.; Lee, S.L.; Jeon, B.G.; Park, B.W.; Rho, G.J. Evaluation of odonto/osteogenic differentiation potential from different regions derived dental tissue stem cells and effect of 17 β -estradiol on efficiency. *BMC Oral. Health.* **2021**, *21*, 15. [[CrossRef](#)]
50. Petrescu, N.B.; Jurj, A.; Sorițău, O.; Lucaciu, O.P.; Dirzu, N.; Raduly, L.; Berindan-Neagoe, I.; Cenariu, M.; Boșca, B.A.; Campian, R.S.; et al. Cannabidiol and Vitamin D3 Impact on Osteogenic Differentiation of Human Dental Mesenchymal Stem Cells. *Medicina* **2020**, *56*, 607. [[CrossRef](#)]
51. Nayak, T.R.; Andersen, H.; Makam, V.S.; Khaw, C.; Bae, S.; Xu, X.; Ee, P.L.; Ahn, J.H.; Hong, B.H.; Pastorin, G.; et al. Graphene for controlled and accelerated osteogenic differentiation of human mesenchymal stem cells. *ACS Nano* **2011**, *5*, 4670–4678. [[CrossRef](#)]
52. Kim, J.; Choi, K.S.; Kim, Y.; Lim, K.T.; Seonwoo, H.; Park, Y.; Kim, D.H.; Choung, P.H.; Cho, C.S.; Kim, S.Y.; et al. Bioactive effects of graphene oxide cell culture substratum on structure and function of human adipose-derived stem cells. *J. Biomed. Mater. Res. A* **2013**, *101*, 3520–3530. [[CrossRef](#)] [[PubMed](#)]
53. Di Carlo, R.; Zara, S.; Ventrella, A.; Siani, G.; Da Ros, T.; Iezzi, G.; Cataldi, A.; Fontana, A. Covalent Decoration of Cortical Membranes with Graphene Oxide as a Substrate for Dental Pulp Stem Cells. *Nanomaterials* **2019**, *9*, 604. [[CrossRef](#)] [[PubMed](#)]
54. Heng, B.C.; Jiang, S.; Yi, B.; Gong, T.; Lim, L.W.; Zhang, C. Small molecules enhance neurogenic differentiation of dental-derived adult stem cells. *Arch. Oral. Biol.* **2019**, *102*, 26–38. [[CrossRef](#)] [[PubMed](#)]
55. Park, D.; Xiang, A.P.; Mao, F.F.; Zhang, L.; Di, C.G.; Liu, X.M.; Shao, Y.; Ma, B.F.; Lee, J.H.; Ha, K.S.; et al. Nestin is required for the proper self-renewal of neural stem cells. *Stem Cells* **2010**, *28*, 2162–2171. [[CrossRef](#)] [[PubMed](#)]
56. Hochuli, A.H.D.; Senegaglia, A.C.; Selenko, A.H.; Fracaro, L.; Brofman, P.R.S. Dental Pulp from Human Exfoliated Deciduous Teeth-derived Stromal Cells Demonstrated Neuronal Potential: In Vivo and In Vitro Studies. *Curr. Stem. Cell Res. Ther.* **2021**, *16*, 495–506. [[CrossRef](#)]
57. Kim, K.S.; Zhao, Y.; Jang, H.; Lee, S.Y.; Kim, J.M.; Kim, K.S.; Ahn, J.H.; Kim, P.; Choi, J.Y.; Hong, B.H. Large-scale pattern growth of graphene films for stretchable transparent electrodes. *Nature* **2009**, *457*, 706–710. [[CrossRef](#)]
58. Reddy, S.; He, L.; Ramakrishana, S.; Luo, H. Graphene nanomaterials for regulating stem cell fate in neurogenesis and their biocompatibility. *Curr. Opin. Biomed. Eng.* **2019**, *10*, 69–78. [[CrossRef](#)]